Titan's haze at opposite seasons from HST-STIS spectroscopy

Titan's haze at opposite seasons from HST-STIS spectroscopy

Erich Karkoschka

Erich Karkoschka, Lunar and Planetary Laboratory, University of Arizona, Tucson, AZ 85721-0092, USA, phone 1 (520) 621-3994, fax 1 (520) 621-4933, e-mail erich@lpl.arizona.edu

Pages: 17

Figures: 5

Tables: 2

Proposed Running Head: Titan's haze at opposite seasons

Highlights:

> HST-STIS image cubes over 22 years provide a unique probe of atmospheric variations.

>Two switches of Titan's two-component north-south asymmetry were observed.

>Both components at each latitude follow remarkably well a harmonic oscillation.

>The low-altitude component lags 2.3 years behind the high-altitude component.

>Our seasonal model fits all data at latitudes to +/- 70 degrees at all eight observed dates.

Key-words: Titan; Titan atmosphere; Atmospheres, structure; Atmospheres, dynamics; Satellites, atmospheres.

Submitted to Icarus: 2022-04-11 Revised: 2022-06-05, 2022-07-11

Abstract

We present an analysis of three new image cubes of Titan by the Space Telescope Imaging Spectrograph taken in 2017, 2018, and 2019, half a Titan year after previously analyzed image cubes. Both data sets probe periods when Titan's seasonal north-south-asymmetry switched. The new observations show that the new reversal came exactly half a Titan year after the previous opposite reversal. On the other hand, the phase lag of the reversals with respect to Titan's equinoxes was different indicating that the seasonal variation is close to harmonic and does not follow variations due to Saturn's orbital eccentricity. The reversal had two components, a major one at altitudes below 80 km reversing two years after a minor one above 150 km. The observations further revealed small temporary deviations of less than 10 % of the seasonal amplitude. The new observations provide an improved seasonal model of Titan that gives accurate constraints for future global circulation models.

Graphical Abstract

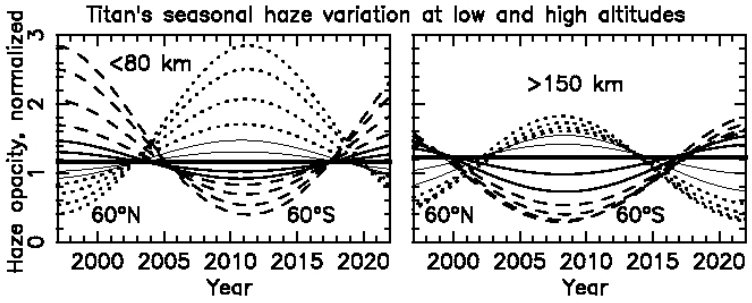

1. Introduction

Titan's atmosphere has a well observed seasonal variation. In 1980 and 1981, the Voyager spacecraft found Titan's atmosphere almost featureless except for a noticeable asymmetry with a bright northern hemisphere and a darker southern hemisphere (Smith *et al.* 1981, 1982). The Hubble Space Telescope (HST) took images at similar wavelengths about two Titan seasons later revealing that the asymmetry had switched (Caldwell *et al.* 1992), consistent with a seasonal change. Photometry of Titan since 1972 at 472 and 551 nm wavelength indicated an almost periodic variation with a period of 15 years, half a Titan year (Lockwood and Thompson 2009). The phase of the variation excluded the possibility of a pure geometric effect due to changing sub-Earth latitudes.

In the 889 nm methane band, HST images of 1990 found the asymmetry to be opposite to that of visible wavelength which was consistent with models by Toon *et al.* (1992) showing that an increase in haze optical depth causes darkening at wavelengths below 600 nm but brightening at longer wavelengths.

Titan's north-south asymmetry has been further explored in wavelength and time through observations from Earth, Earth orbit, and Cassini. Ground-based telescopes with adaptive optics were among the first to measure the north-south asymmetry in greater spatial detail (Coustenis *et al*., 2001; Roe *et al*., 2002, Ádámkovics *et al*., 2006). Cassini followed with much better resolution (de Kok *et al*., 2010; Penteado *et al*., 2010; Teanby *et al*., 2012; Vinatier *et al*., 2015). HST contributed significantly to record the temporal evolution of the asymmetry because its observations are not affected by the varying seeing or atmospheric transmission of ground-based telescopes and almost neither by the varying phase angle of Cassini observations.

Observations by the Space Telescope Imaging Spectrograph (STIS) gave more complete spectral characterizations than HST imaging in a few filters (Karkoschka and Lorenz 1996; Lorenz *et al*., 2006) since STIS can obtain image cubes with 1024 wavelengths of the whole disk of Titan at full spatial resolution within one orbit around Earth. Such image cubes were taken in 1999 and 2000, also in 2002 with less s spatial resolution. Furthermore, partial image cubes were obtained in 1997 and 2004. These five image cubes were analyzed by Karkoschka (2016). Their superb spectral information revealed that the north-south asymmetry is caused by two distinct cycles. The major cycle involves low altitudes (<80 km) with a north-south switch occurring in 2003-2004, a 90° phase lag with respect to Titan's fall equinox in 1995. The minor cycle

involves high altitudes (>150 km) with a switch occurring in 2001-2002, corresponding to a smaller phase lag.

In this work, we analyze new STIS image cubes of the full disk at full spatial resolution taken in 2017, 2018, and 2019. They record the opposite switch, including the timing and speed during the switch. Both data sets were reduced in the same way in order to detect fine differences. The following Section 2 explains the new observations and data reduction. Only a summary is given since the details were listed in Karkoschka (2016). Section 3 details the modeling and comparison with the previous data. Section 4 provides a summary.

2. Data reduction

HST took new images cubes of Titan with STIS in 2017, 2018, and 2019 (Table 1). The G750L grating provided wavelengths between 532 and 1016 nm at 0.49 nm/pixel over 1024 pixels. The slit width was 0.05 arc-sec. The spatial sampling was 0.05 arc-sec/pixel along the slit, providing up to 16 pixels across the disk of Titan. Spatial sampling perpendicular to the slit was accomplished through 15-16 exposures in each year separated by 0.05 arc-sec. Fig. 1 shows the slit locations on Titan's disk according to our calibration.

Table 1: Observational parameters

Date, UT	L_s (°)	lg(earth) (º)	φ(earth) (º)	φ(sun) (º)	diameter (arc-sec)	phase angle (º)	# of exposures
2017-05-17.72	90	225	26.5	26.8	0.775	2.8	16
2018-06-08.79	102	312	25.7	26.1	0.780	1.9	16
2019-08-10.52	115	240	24.9	24.1	0.774	3.1	15

Note: lg and φ are sub-earth/sub-solar longitudes and latitudes, respectively. L_s is the solar longitude relative to the spring equinox.

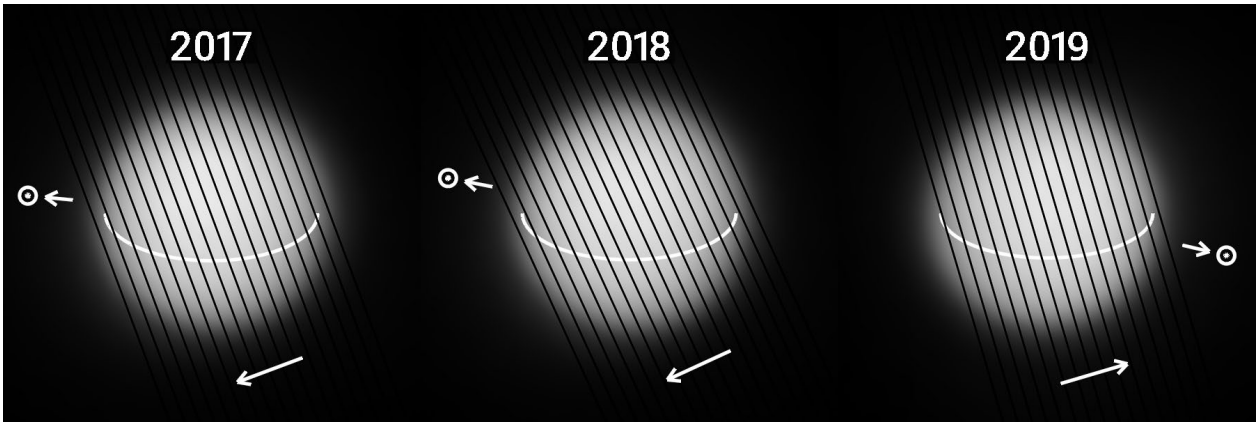

Fig. 1: The geometry for all slit positions on Titan's disk, shown for each observing date. North on Titan is oriented upwards in each image. Titan's equator is shown by the bright curve. The direction to the sun is also shown. The arrows at the bottom give the direction of offset of the slit from one exposure to the next. Even the only 15 slit positions in 2019 provided very close to complete coverage of Titan's disk.

The observations were placed near the edge of the CCD (aperture 52X0.05E1) to minimize charge-transfer losses. After spatial and wavelength calibration of each data point to about 0.002 arc-sec and 0.03 nm, each image cube was resampled at 0.06 Titan-radii and 0.4 nm wavelength. Separate deconvolutions were done for the CCD scattering and the telescope diffraction.

The ~1000 spectral data points were divided into 25 groups of about 40 spectral points each that varied little in wavelength and methane absorption coefficient (top of Fig. 2). These 25 groups had eight different average wavelengths and eight different average methane absorption coefficients. This allowed us to see how Titan's reflectivity changes with wavelength at constant methane absorption coefficient and vice versa.

This work focuses on Titan's atmosphere, but the data also probe its surface, in particular at low methane absorptions and long wavelengths (Fig. 2). The visible features correspond well with Cassini ISS map PIA22770 (https://photojournal.jpl.nasa.gov/catalog/PIA22770) when generated for the same viewing angle and spatial resolution (right column in Fig. 2). For each spectral band, the correlation with the ISS map was determined which then allowed us to subtract the surface features.

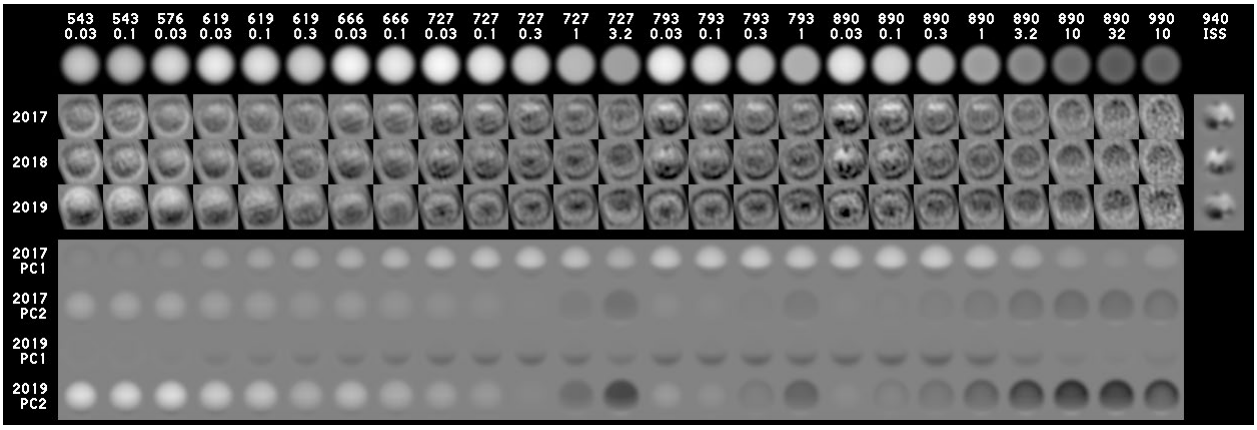

Fig. 2: Titan images for our 25 spectral bands, combinations of central wavelength and methane absorption coefficient listed on top, and three observing sessions listed on the left side. To better display small variations, an average intensity distribution shown in the top row was subtracted before the difference was displayed with quadruple contrast. The column at right shows Titan surface albedo features measured by Cassini ISS. The bottom four rows show contributions from the first two principal components to Titan's disk reflectivity in 2017 and 2019.

Titan's disk was divided into 10 latitude regions separated by 10°, centered on 25° South up to 65° North. In each latitude region the reflectivity data points were fit to a linear function with the cosine of emission angle. The fitted reflectivities at cosines of 0.6 and 0.8 represent two parameters, such as reflectivity and limb darkening, that were used to compare data at different latitudes and different times.

In summary, we reduced the data from about 600,000 original data points to 1500 data points: 25 spectral bands, 10 latitudes, two center-to-limb locations, and three observing dates.

3. Principal component analysis

We applied the same method of principal component analysis that was used for the STIS observations of 1997-2004 (Karkoschka 2016). While the 1500 reflectivity data points are functions of four parameters (spectral band, latitude, center-to-limb position, time), the method tries to fit the data as it were the product of two functions, a function A1 only dependent on spectral band and center-to-limb position and a function B1 only dependent on latitude and time. The function A1 describes a physical variation in Titan's atmosphere, such as a change of optical depth below 80 km altitude. The function B1 describes the magnitude of this change as function

of latitude and time. Note that the average state of Titan was subtracted from all data points so that the principal component analysis only deals with deviations from the average state.

$$I/F(\lambda,\mu,\varphi,t) = I/F_{\text{average}}(\lambda,\mu) + A1(\lambda,\mu)\, B1(\varphi,t) + A2(\lambda,\mu)\, B2(\varphi,t) + \ldots \quad (1)$$

where I/F is the reflectivity, λ the wavelength, μ the center-to-limb position, φ the latitude, and t the time.

Since the first principal component, the product of A1 and B1, only approximates the data to about 70 %, the residuals are fitted with the second principal component, the product of functions A2 and B2, which explains another ~25 % of the variation in the data. The remaining principal components are due to noise, imperfections of the surface feature subtraction, or very small physical variations. The third principal component may be related with a non-linearity of the first principal component (Karkoschka 2016).

The 2.2 year time period of the new observations is too short to describe seasonal variations with a period of 29.5 years accurately. Thus, we added the previous STIS observations of 1997-2004 to the data set, which gave almost identical first and second principal components as using the previous data set alone. This means that the conclusions about the physical nature of both components stand firm, mainly that the first component corresponds to a variation of the haze optical depth below 80 km altitude, and the second one above 150 km altitude.

Karkoschka (2016) showed that the structure of the 50 data points each of A1 and A2 (25 spectral bands for two center-to-limb positions) match radiative transfer models of Titan's atmosphere best if the haze optical depth is varied and all other parameters remain constant, and that A1 is best approximated if the optical depth is varied between 0 and 80 km altitude, and A2 similarly for altitudes above 150 km. We used the Titan's haze model from Doose *et al.* (2016) for the Huygens landing site during the descent of Huygens. It divides the atmosphere into four layers: above 200 km, then down to 80 km, to 30 km, and below. Each layer has its own aerosol size with phase functions derived from fractal particles, high single scattering albedos, up to unity at 800 nm wavelength and low altitudes, and its own function of optical depth with altitude, depending strongly on wavelength. The haze optical depths determined in this work at a certain latitude and time divided by the haze optical depth in the Doose et al. model is called the *haze opacity factor*, which is unity between 80 and 150 km altitude. Single scattering albedos and phase functions are from Doose *et al.* without change.

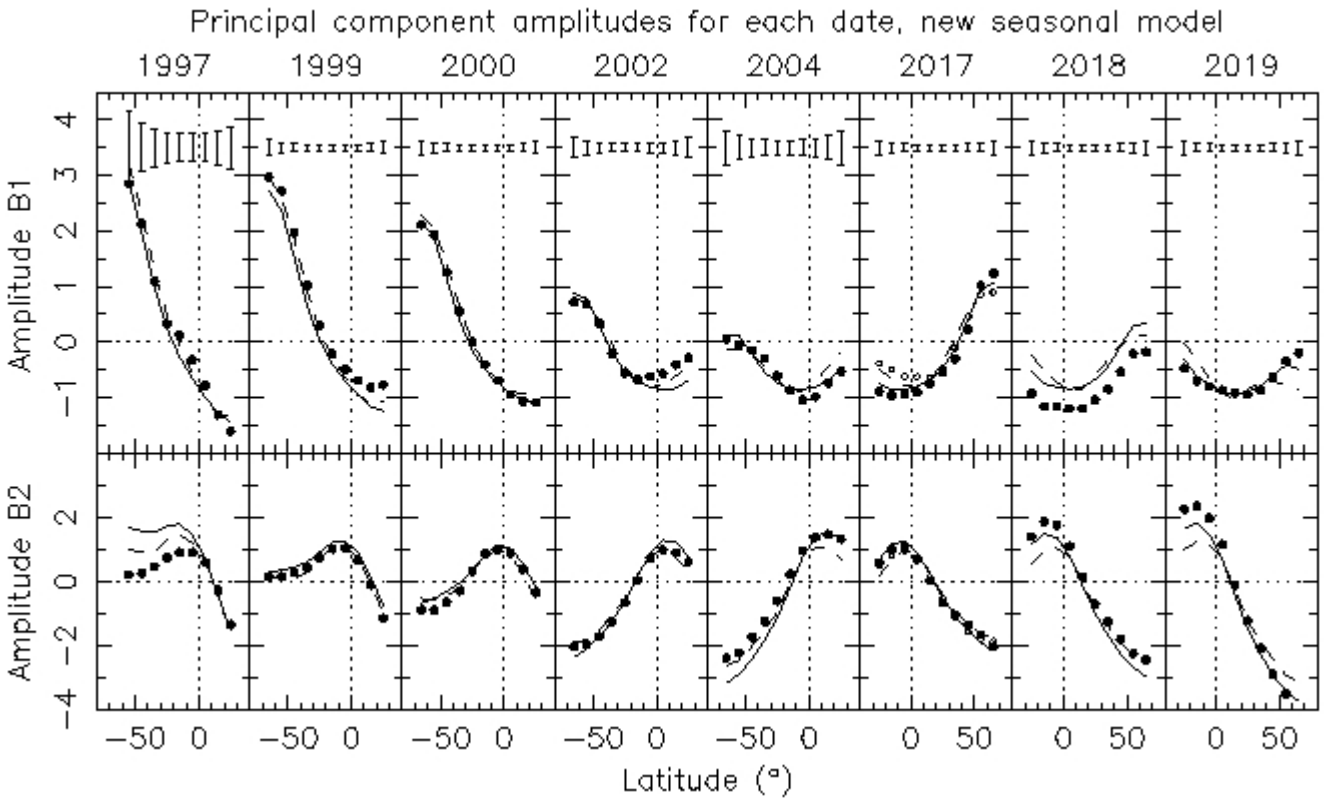

171
172

173 Fig. 3: Principal component values $B1$ (top) and $B2$ (bottom), ordered first according to
174 observing date (top of each panel), and then according to latitude (bottom scale). Error bars are
175 indicated at the top. Curves are for the seasonal model of Karkoschka (2016, dashed) and the
176 new seasonal model of this work (solid). The small circles in the 2017 panel are a prediction
177 from data half a Titan-year earlier, an interpolation between the 2000 and 2002 observations,
178 with north and south reversed.

We also note that the seasonal model of Titan's haze by Karkoschka (2016) using the 1997-2004 observation predicts the new observations reasonably well, which is our first result (dashed curves in Fig. 3). Another comparison is shown in the panel of the 2017 observations, where the 2017 observations (dots) are compared with the expected ones from half a Titan-year earlier (crosses). The fit is remarkably good, especially for the second principal component. This is the best suitable comparison at opposite seasons since the 2004 observations are less reliable due to their incomplete coverage of Titan's disk. Note that the adopted seasonal model gives the reverse latitudinal distribution after half a Titan year, an assumption that could be far off. The new observations show that this assumption was quite good for the 2002 versus 2017 comparison.

The seasonal model does not fit the 2018 and 2019 observations as well as those of other years. There are at least three possibilities. First, Titan may change periodically but somewhat differently at opposite seasons, such as changing at faster speeds around 2018 than around 2003. Second, every change may have their individual signature. Third, Titan changes symmetrically at opposite seasons, but the opposite season of the previous period ended in 2018 and the extrapolation to 2019 was not accurate. We found that the third possibility is likely the correct explanation.

We did a new seasonal model using a least square method with all data points. It fits the 2018 and 2019 data better without making the fit to the other data significantly worse (solid curves in Fig. 3). The 1997 and 2004 observation are not fit as well, but those data are unreliable since they only cover part of Titan's disk. This was a weakness of the previous data set. Thus, we could improve our model because the 2019 observations extend the temporal baseline even when accounting for the anti-symmetry after 14.7 years. The parameters of the principal components B1 and B2 are listed in Table 2. The seasonal model describes B1 and B2 as function of latitude φ and time *t* (in years):

$$Bi(\varphi,t)= Mi(\varphi) + Di(\varphi) \sin [(t - Ei(\varphi)) \, 2\pi/29.46] \quad (2)$$

The 42 parameters of the seasonal model are displayed in Fig. 4.

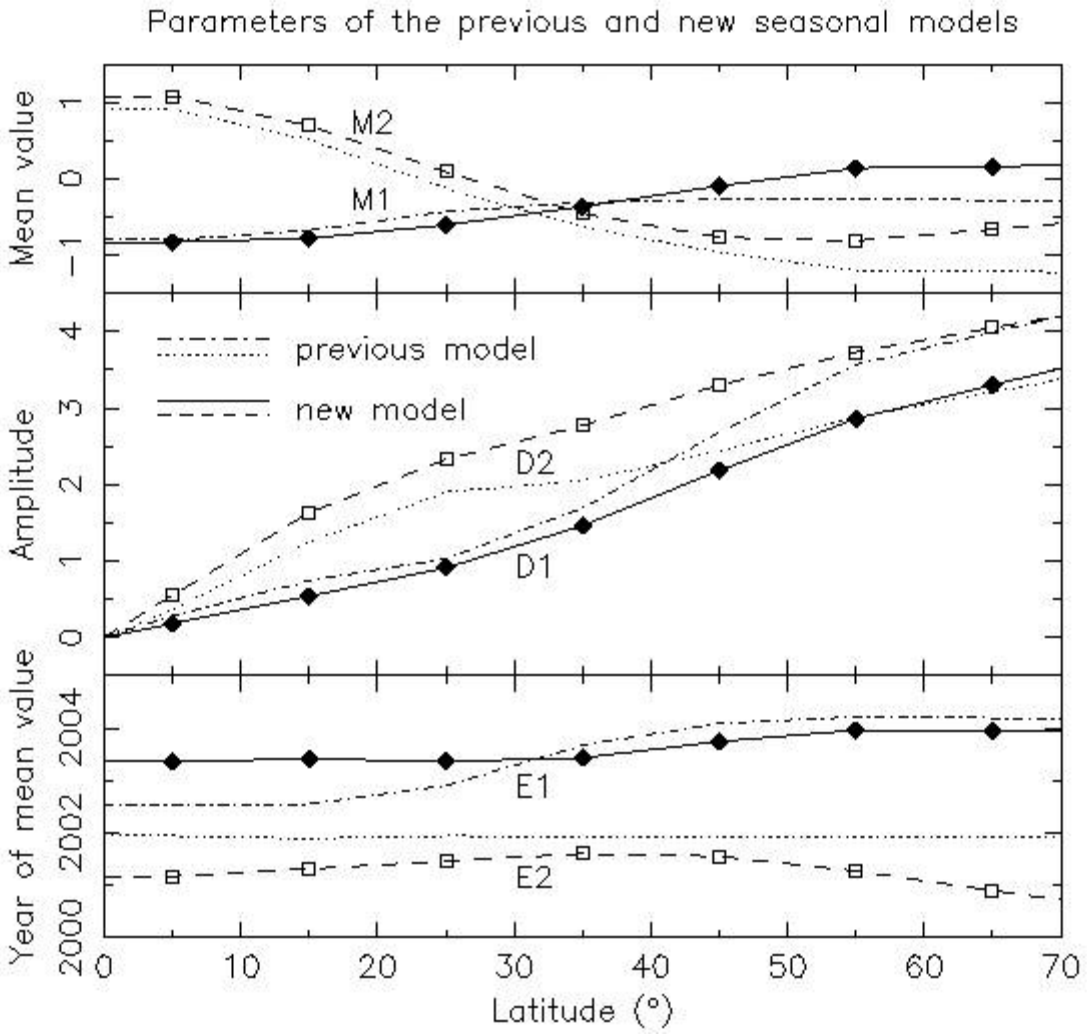

206

207 Fig. 4: The three parameters of the seasonal model for the first (solid dot and curves) and second
208 principal component (open squares and dashed curves), each as function of latitude according to
209 Eq. 2. Southern latitudes are assumed symmetric to northern ones, except for a change of sign
210 for *D*1 and *D*2.

Table 2: Principal component values B1 and B2

	B1			B2		
Latitude	2017	2018	2019	2017	2018	2019
-25°	-0.89	-0.93	-0.47	0.58	1.40	0.25
-15°	-0.96	-1.16	-0.71	0.99	1.87	2.35
-5°	-0.94	-1.16	-0.80	1.08	1.76	1.98
5°	-0.90	-1.20	-0.87	0.70	1.10	1.16
15°	-0.75	-1.20	-0.87	0.03	0.15	-0.11
25°	-0.54	-1.04	-0.95	-0.65	-0.70	-1.20
35°	-0.31	-0.85	-0.87	-1.05	-1.25	-2.06
45°	0.23	-0.54	-0.62	-1.35	-1.78	-2.87
55°	1.02	-0.21	-0.34	-1.64	-2.23	-3.47
65°	1.24	-0.18	-0.20	-2.01	-2.43	-4.18

The seasonal model has the reversal for the first principal component (low altitudes) occurring during 2003 (2003.6±0.2), consistent with Karkoschka (2016), but the second principal component (high altitudes) seems to switch in early 2001 (2001.3±0.2) rather than late 2001 suggested from the more limited earlier data set. This gives a phase shift of 2.3±0.3 years between both oscillations. The phase lags of the first and second principal component with respect to Titan's seasons are 91° and 63°, respectively. These numbers correspond to Saturn's mean motion around the sun, ignoring the orbital eccentricity. The apparent variations of the reversal times with latitude are close to the expected uncertainty and probably not significant.

The new seasonal model in terms of haze opacity factor at low and high altitude is shown in Fig. 5 for all investigated latitudes. The new constraints at opposite seasons make the model more reliable. However, one still needs to consider that STIS never observed Titan around the equinoxes, which means that the seasonal model is an extrapolation based on the assumption of harmonic oscillations. Also, high southern latitudes cannot be observed from Earth around Titan's northern summer solstice, and the same holds true for high northern latitudes near the winter solstice. The seasonal model may not be accurate there.

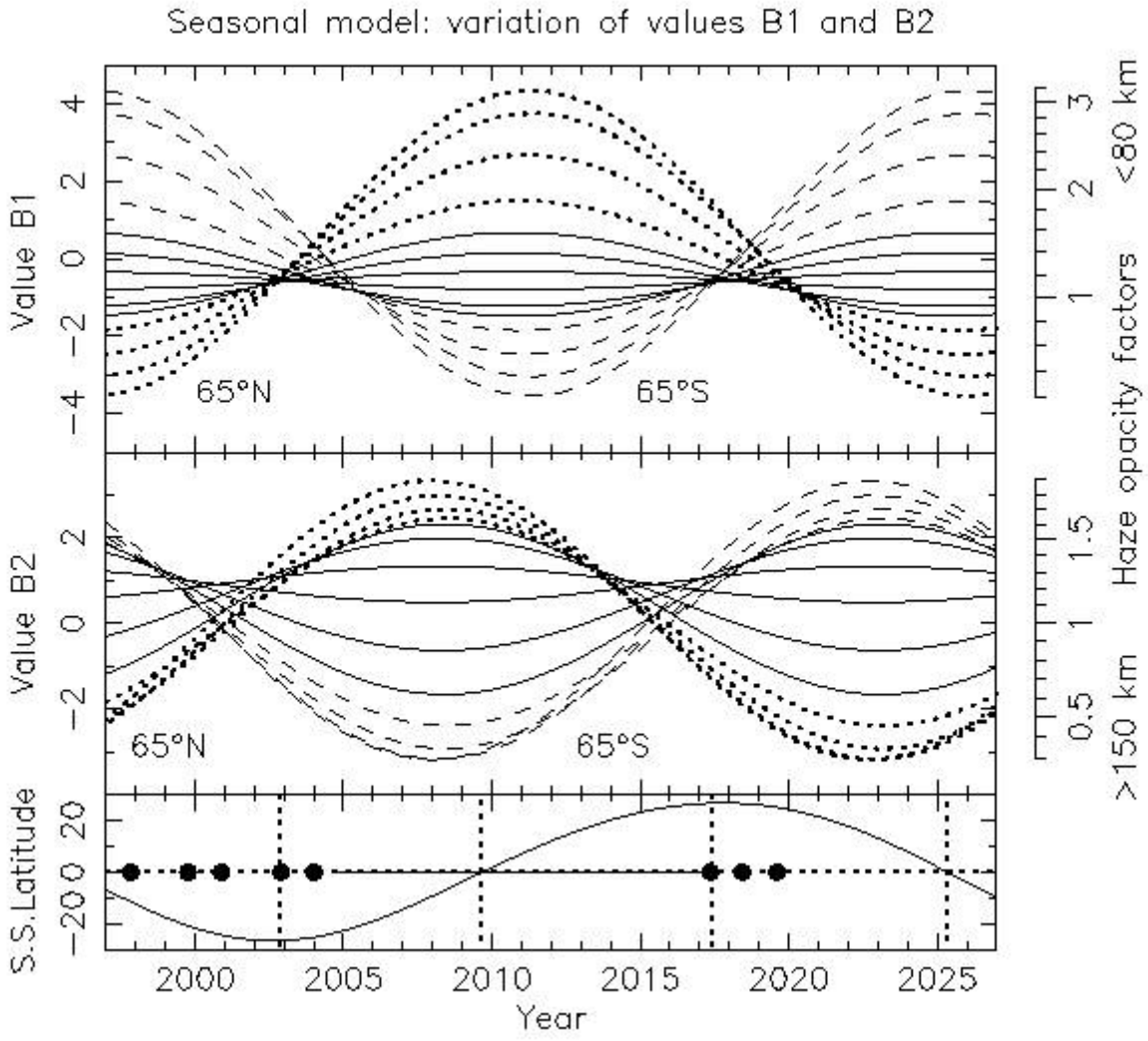

Fig. 5: The variation of values *B*1 (top) and *B*2 (middle) as function of time over a whole Titan year for 14 latitudes from -65° to 65° latitude, every 10°. The six latitudes within 30° of the Equator are shown as solid curves, the ones further north and south as dotted and dashed, respectively. The bottom panel shows the sub-solar latitude. The eight dots indicate the dates for our observations, the horizontal bar the duration of the Cassini mission at Saturn, and the vertical dotted lines the equinoxes and solstices. The scales at the right show approximate haze opacity factors for altitudes below 80 km (top panel) and above 150 km (middle panel).

We wanted to test whether Titan's eccentricity causes a non-harmonic oscillation in the atmospheric response. The duration from fall equinox in 1995 to spring equinox in 2009 is 13.7 years while the following duration to the next fall equinox in 2025 is 15.7 years. This might suggest that the reversals of the north-south asymmetry around 2017 occur 13.7 years after those

around 2003. However, allowing for a non-harmonic contribution, our analysis gives best fits of 14.5±0.3 years between reversals for the low altitude variation and 14.7±0.3 years for the high-altitude variation. Both values are consistent with half a Titan year of 14.7 years but inconsistent with the 13.7 years guessed above. This result might be expected considering the long phase lags of both variations, especially the low altitude change. Long phase lags usually indicate a system that has little response to forcing of higher frequencies. Titan's eccentricity effectively adds a small contribution of a second harmonic to the first harmonic.

If the second harmonic is shifted by half a season, the time between reversals remains half a Titan year, but the speeds near both reversals are different. Again, there is no evidence in the data set for this. An added second harmonic does not decrease residuals.

Seasonal variations such as in Equation (2) can also be expressed as a function of Saturn's orbital longitude, often with zero longitude defined as Titan's spring equinox. We tried this and found the residuals to be 5 % larger than when using time as in Equation (2). The fact that residuals are similar can be expected since the difference between both curves is small around the solstices where we have data. The fact that eccentricity does not seem to matter may also be expected because the phase lags are large. The system is responding roughly to the average solar illumination over the last two seasons, not particularly to the illumination at the time of observation.

We detected small but significant short-lived deviations from the harmonic oscillations at certain latitudes and times. The most significant deviation occurred in June 2018 (Fig. 3) when the observed state at low altitudes (principal component 1) had an optical depth lower by 10 % of the seasonal amplitude or 5 % of the maximum minus minimum. This is somewhat comparable to the photometry data by Lockwood and Thompson (2009) that also showed that small, irregular deviations from the harmonic oscillation occur. These short-term deviations do not repeat itself after a cycle. Each cycle has a slightly different shape. Variations of the haze opacity of comparable magnitude, 5-10 %, and time scales of weeks to months were tracked by Nichols-Fleming *et al.* (2021). The presence of these short-term variations limits the accuracy of determining seasonal variations based on a handful of observation dates.

4. Summary

Titan's north-south asymmetry has been observed for decades with various instruments.

One of the best data sets describing the asymmetry comes from STIS image cubes at ~1000 wavelengths between 520 and 1020 nm. Images cubes in five of the years 1997-2004 revealed that the north-south asymmetry is a superposition of two distinct variations, a low-altitude variation causing most of the observed changes and a high-altitude variation contributing (Karkoschka 2016). Both are seasonal variations with the period of a Titan year, but the low-altitude variation is two years behind the high-altitude variation in phase.

New STIS image cubes taken in 2017, 2018, and 2019 captured the reversals of both variations at the opposite season compared to the earlier image cubes. They were specifically designed for the goal of this investigation and thus cover the whole disk of Titan at full resolution. For the previous STIS image cubes, this was only true for two years out of five since those observations had other goals. The full set of eight image cubes was analyzed here.

Our main result is that the seasonal model based on the previous image cubes (Karkoschka 2016) predicted the new observations remarkably well. This is even true for high northern latitudes that were not observable in the previous image cube. Their seasonal model was inferred based on symmetry with respect to the equator except for a phase shift of half a Titan year. This means that both variations at low and high altitudes can be well approximated by a simple harmonic, seasonal variation.

We tested whether the seasonal variation can be better approximated by a slightly non-harmonic oscillation that accounts for the variable orbital speed of Saturn due to its orbital eccentricity which affects the timing of Titan's seasons. We found that the observed seasonal variation is not significantly affected by the finite eccentricity and much better approximated by pure harmonic oscillations. Since we only tried the simplest deviations from a harmonic oscillation, we cannot say whether more sophisticated variations might better fit the data.

The amplitudes of the seasonal variation at both altitudes increase almost perfectly linearly with latitude up to about 70° North and South. This is consistent with measurements based on only the earlier image cubes.

For the annual average of Titan's haze opacity, the first principal component (low-altitude variation) has slightly lower values at the equator than at high latitudes while this is opposite for the second principal component (high-altitude variation). This was also suggested already from the first five image cubes alone.

The phase lags of the variation of Titan's haze opacity with respect to Titan's seasons is

91° at low altitudes (<80 km) and 63° at high altitudes (>150 km). The difference of 28° corresponds to a relative delay of 2.3±0.3 years, a little more than the almost 2 years determined from the previous smaller data set. The new value is more reliable.

Our data is limited to two periods around Titan's solstices. Thus, our seasonal model may be wrong around the equinoxes. Around the solstices, the tropics can be probed well from Earth, but higher latitudes only on the summer hemisphere. Thus, our seasonal model may be also wrong at higher latitudes around the winter solstice. Cassini data show a large polar cloud in the winter hemisphere extending to mid-latitudes (Le Mouélic *et al.*, 2018) that is clearly different from our seasonal model, although our seasonal model at altitudes above 150 km has the largest opacity during the winter, a qualitative agreement at least.

We detected small, short-lived deviations from the otherwise smooth, seasonal cycle, up to about 10 % of the amplitude of the seasonal cycle. They may be comparable to weather modifying the seasonal cycle on Earth.

The whole set of STIS observations provides some details of both seasonal variations, in particular of the haze opacity at altitudes of <80 km and >150 km, the amplitudes, the phase shift between both variations of 2.3 years, and the seasonal averages as function of latitude. They all give constraints that can improve global circulation models of Titan (Rannou *et al*., 2004; Crespin *et al.*, 2008; Lora *et al.*, 2015, 2019).

Acknowledgements

This work was supported by the STScI through General Observer program GO 14612. Support for HST was provided by NASA through the Space Telescope Science Institute, which is operated by the Association of Universities for Research in Astronomy, Incorporated, under NASA contract NAS5-26555.

References

Ádámkovics, M., de Pater, I., Hartung, M., Eisenhauer, F., Genzel, R. 2006. Titan's bright spots: multiband spectroscopic measurement of surface diversity and hazes. *J. Geophys. Res.* **111**, E07S06.

Brown, R.H., and 25 colleagues 2006. Observations in the Saturn system during approach and orbital insertion, with Cassini's visual and infrared mapping spectrometer (VIMS). Astron. *Astrophys.* **446**, 707-716.

Caldwell, J.D., Smith, P.H., Tomasko, M.G., McKay, C.P. 1992. Titan: evidence of seasonal change—A comparison of Voyager and Hubble Space Telescope images. *Icarus* **103**, 1-9.

Coustenis, A., Gendron, E., Lai, O., Véran, J.-P., Woillez, J., Combes, M., Vapillon, L., Fusco, T., Mugnier, L., Rannou, P. 2001. Images of Titan at 1.3 and 1.6 μm with adaptive optics at the CFHT. *Icarus* **154**, 501-515.

Crespin, A., Lebonnois, S., Vinatier, S., Bézard, B., Coustenis, A., Teanby, N.A., Achterberg, R.K., Rannou, P., Hourdin, F. 2008. Diagnostics of Titan's stratospheric dynamics using Cassini/CIRS data and the two-dimensional IPSL circulation model. *Icarus* **197**, 556-571.

de Kok, R., Irwin, P.G.J., Teanby, N.A., Vinatier, S., Tosi, F., Negrão, A., Osprey, S., Ardiani, A., Moriconi, M.L., Coradini, A. 2010. A tropical haze band in Titan's stratosphere. *Icarus* **207**, 485-490.

Karkoschka, E., Lorenz, R.D. 1996. Latitudinal variation of aerosol sizes inferred from Titan's shadow. *Icarus* **125**, 369-379.

Karkoschka, E. 2016. Seasonal variation of Titan's haze at low and high altitudes. *Icarus* **270**, 339-354.

Le Mouélic S., Rodriguez, S., Robidel, R., Rousseau, B., Seignovert, B., Sotin, C., Barnes, J.W., Brown, R.H., Baines, K.H., Buratti, B.J., Clark, R.N., Nicholson, P.D., Rannou, P., Cornet, T. 2018. Mapping polar atmospheric features on Titan with VIMS: from the dissipation of the northern cloud to onset of a southern polar vortex. *Icarus* **311**, 371-383.

Lockwood, G.W., Thompson, D.T. 2009. Seasonal photometric variability of Titan, 1972-2006. *Icarus* **200**, 616-626.

Lora, J.M., Lunine, J.I., Russell, J.L. 2015. GCM simulations of Titan's middle and lower atmosphere and comparison to observations. *Icarus* **250**, 516-528.

Lora, J.M., Tokano, T., Vatant d'Ollone, J., Lebonnois, S., Lorenz, R.D. 2019. A model intercomparison of Titan's climate and low-altitude environment. *Icarus* **333**, 113-126.

Lorenz, R.D., Lemmon, M.T., Smith, P.H. 2006. Seasonal evolution of Titan's dark polar hood: midsummer disappearance observed by the Hubble Space telescope. *Monthly Notices Royal Astron. Soc.* **369**, 1683-1687.

Nichols-Fleming, F., Corlies, P., Hayes, A.G., Ádámkovics, M., Rojo, P., Rodriguez, S., Turtle, E.P., Lora, J.M., Soderblom, J.M. 2021. Tracking short-term variations in the haze distribution of Titan's atmosphere with SINFONI VLT. *Planetary Science J.* **2**:180.

Penteado, P.F., Griffith, C.A., Tomasko, M.G., Engel, S., See, C., Doose, L., Baines, K.H., Brown, R.H., Buratti, B.J., Clark, R., Nicholson, P., Sotin, C. 2010. Latitudinal variations in Titan's methane and haze from Cassini VIMS observations. *Icarus* **206**, 352-365.

Rannou, P., Hourdin, F., McKay, C.P., Luz, D. 2004. A coupled dynamics-microphysics model of Titan's atmosphere. *Icarus* **170**, 443-462.

Roe, H.G., de Pater, I., Macintosh, B.A., Gibbard, S.G., Max, C.E., McKay, C.P. 2002. Titan's atmosphere in late southern spring observed with adaptive opticson the W. M. Keck II 10-meter telescope. *Icarus* **157**, 254-258.

Smith, B.A., Soderblom, L.A., Beebe, R., Boyce, J., Briggs, G., Bunker, A., Collins, S.A., Hansen, C.J., Johnson, T.V., Mitchell, J.L., Terrile, R.J., Carr, M., Cook II, A.F., Cuzzi, J., Pollack, J.B., Danielson, G.E., Ingersoll, A., Davies, M.E., Hunt, G.E., Masursky, H., Shoemaker, E., Morrison, D., Owen, T., Sagan, C., Veverka, J., Strom, R., Suomi, V. 1981. Encounter with Saturn: Voyager 1 imaging results. *Science* **212**, 163-182.

Smith, B.A., Soderblom, L.A., Batson, B., Bridges, P., Inoe, J., Masursky, H., Shoemaker, E., Beebe, R., Boyce, J., Briggs, G., Bunker, A., Collins, S.A., Hansen, C.J., Johnson, T.V., Mitchell, J.L., Terrile, R.J., Carr, M., Cook II, A.F., Cuzzi, J., Pollack, J.B., Danielson, G.E., Ingersoll, A., Davies, M.E., Hunt, G.E., Morrison, D., Owen, T., Sagan, C., Veverka, J., Strom, R., Suomi, V. 1982. A new look at the Saturn system: The Voyager 2 images. *Science* **215**, 504-537.

Teanby, N.A., Irwin, P.G.J., Nixon, C.A., de Kok, R., Vinatier, S., Coustenis, A., Sefton-Nash, E., Calcutt, S.B., Flasar, F.M. 2012. Active upper-atmosphere chemistry and dynamics from polar circulation reversal on Titan. *Nature* **491**, 732-735.

Vinatier, S. Bézard, B., Lebonnois, S., Teanby, N.A., Achterberg, A.K., Gorius, N.,

404 Mamoutkine, A., Guandique, E., Jolly, A., Jennings, D.E. Flasar, F.M. 2015. Seasonal variation
405 in Titan's middle atmosphere during the northern spring derived from Cassini/CIRS observations.
406 *Icarus* **250**, 95-115.